Parametric numerical study of Savonius wind turbine interaction in a linear array

R. Mereu*, D. Federici, G. Ferrari, P. Schito, F. Inzoli

Politecnico di Milano, Piazza Leonardo da Vinci 32, 20133 Milano, Italy

This work focuses on Savonius turbine numerical modeling and mutual turbine interaction in a linear array farm. Two-dimensional Computational Fluid Dynamics modeling was carried out using the open source solver OpenFOAM. Results are compared with available experimental data and three-dimensional CFD modeling. The influence of main parameters, such as the distance between adjacent turbines, the wind incidence angle and the number of turbines is investigated and the linear array efficiency is defined. The obtained results show a performance increase as the distance between the turbines reduces, higher efficiency for small wind incidence angles, and a larger number of turbines.

Keywords: Vertical axis wind turbine (VAWT) Savonius, Computational Fluid Dynamics (CFD) Wind angle, Turbine distance, Farm size

1. Introduction

In recent years, the attention on sustainable electricity generation has grown because of the uncontrolled exploitation of non-renewable energy resources and related issues, such as supply security and environmental pollution. The consequence has been increasing attention to energy issues, seeking alternative renewable sources such as wind, solar, biomass or tidal energy. In this path of change, also the scale of power generation plants has been subjected to revision, passing from pure centralized generation in large power plants to smaller ones distributed throughout the territory. Focusing on wind energy conversion, the typical power plant is composed of several wind turbines installed in an appropriate way to maximize the global energy production, with the name of wind farm. The most efficient wind energy harvesting method consists in the use of horizontal axis wind turbines (HAWTs), that in the last years have been developing towards larger diameters (up to 160 m) and larger power production (up to 10 MW) [1]. These are very large machines that require complex design criteria and control solutions to work and resist all wind conditions: the turbine must follow the incoming wind direction, the blades must be pitched to maximize energy harvesting or to reduce the loads on the structure.

Vertical axis wind turbines (VAWT) are generally simpler devices, since there is no need to align the turbine with the incoming wind direction. The generation of power, however, is unstable if particular design solutions are not taken into account, as described by Vaughn [2]. The main issue for VAWTs is the fixing of the turbine to the ground through the main shaft: all the aerodynamic actions are supported by the bearing, that may also be a source of energy dissipation through friction. Darrieus VAWTs are lift driven wind turbines, achieving a relatively efficient energy harvest, but their main drawback is that they have no self-starting capabilities. A wind detection device and a starting motor are hence necessary.

A Savonius configuration is the simplest wind harvesting device, since it needs no yawing control and has self-starting capabilities. It also provides the lowest efficiency, due to the fact that power production is substantially generated by drag. In the new condition of micro-generation, the use of wind energy through a turbine of the Savonius type could represent a reliable, simple and economically competitive solution. This particular turbine has a high starting torque (Sivasegaram et al. [3]), and can operate under complex turbulent flows (Pope et al. [4]). Recent studies have been performed to assess the performance of lift-driven VAWTs [5–7] and draft-driven Savonius [8,9] turbines using experimental and

Article history:
Received 17 February 2017
Received in revised form
27 June 2017
Accepted 28 June 2017
Available online 1 July 2017

* Corresponding author.
E-mail address: riccardo.mereu@polimi.it (R. Mereu).

Published Journal Article available at: http://dx.doi.org/10.1016/j.renene.2017.06.094

Computational Fluid Dynamics (CFD) approaches: the flow structure is very complex, with strong variations related to the turbine operating conditions and aspect ratio.

An important role for wind turbine efficiency is played by wake interaction in multiple turbine arrangement (i.e. array and wind farm). The distance between adjacent turbines has been widely studied for HAWTs, defining a minimum distance equal to 5 turbine diameters (5*D*), to limit excessive wake influences, even if the wake region extends for more than 5D in both onshore and offshore applications [10,11]. As the distribution of turbines out of the wake influence is not feasible, they are placed in a configuration able to guarantee the maximum distance in the direction of the local dominant wind and at a reduced distance in directions with less wind or perpendicular to the dominant one. Configurations with a linear array of turbines have shown energy generation losses up to 55–60% in HAWT farms [12], with an evident influence of turbine spacing, terrain and environmental conditions on flow recovery. In the case of a linear array of turbines aligned with the wind, the wakes of the upstream turbines are passed down the row, with the first downstream turbine mainly penalized by a decrease in the centreline flow velocity, whereas the remaining downstream turbines are significantly less impacted [13].

Lift-driven VAWT arrays have been recently studied, focusing on spatial farm extension, wind free-stream velocity and the direction of turbine rotation [14–17].

Dabiri [14] and Kinzel [15] studied two-VAWT configurations, observing a small performance increase using counter-rotating turbines, in comparison with a one-turbine installation. Dabiri and Kinzel found similar results, with the downstream turbine recovering up to 95% of the wind free-stream velocity when the streamwise distance was 4-6*D*, while at the same operating conditions, the HAWT requires up to 15-20*D* to recover the same velocity.

Duraisamy et al. [16] studied the flow behavior and performance of VAWT arrays using a two-dimensional CFD numerical approach. Results show that most of the velocity decrease is spatially limited to a few diameters downstream of turbine, diminishing with increased rotational speed. The wake deficit effect increases further downstream in linear array configuration (i.e. straight single row), independently from the direction of rotation of the individual turbines. They also studied the aerodynamic interference between adjacent turbines, which can produce regions with an excess of momentum between the turbines and, in multiple row configurations, a higher efficiency of the downstream rows compared to the leading one, when spaced optimally.

Finally, Ahmadi-Baloutaki et al. [17] performed a wind tunnel test comparing different two- and three-turbine wind-perpendicular configurations with a single-turbine installation. Tests show that the single turbine energy output is very close for all configurations, indicating that turbine performance is not affected by neighboring turbine(s), as observed in HAWT farms for the same turbine distances. Counter and co-rotating pairs, the most commonly installed configuration in VAWT farms, show the same increase in power output, with a turbine spacing of 1*D* and moderate free-stream wind velocity (14 m/s). Co-rotating configuration shows a power coefficient decrease, reaching a value lower than single turbine configuration, as the free-stream velocity increases. This is explained by authors through the modification of the bulk velocity, with respect to low and moderate velocity cases.

These studies show how, in general, lift-driven VAWTs can perform better than HAWTs in farm configurations, with less turbine distances in both perpendicular and parallel wind direction with respect to turbine distribution. Furthermore, independently from counter and co-rotating configurations, the flow can recover free-stream velocity downstream of the turbine and related turbine efficiency, with very reduced distances, when compared to HAWT farms.

Several studies via experimental, theoretical and numerical approaches are present in literature, showing that different arrangements of Savonius turbines have significantly different behaviors. The disadvantage of this technology is lower power and efficiency compared to lift-driven turbines. Previous studies have shown that it is possible to achieve efficiency improvements from turbine mutual interaction [18–20]. In literature, the interaction between turbines is mainly investigated via a numerical approach. Mohammed et al. [21] analyzed a cluster with two and three turbines, varying several factors such as inter-axial distance, wind incidence angle and rotation direction of the turbines. Generally, data present in literature are related to clusters composed of two or at most three turbines (El-Baz et al. [22]), arranged in different configurations.

Savonius wind turbines can represent a valid alternative solution for distributed power generation in urban areas, where available space is a key factor and imposes several limitations to farm design. To improve the understanding of Savonius wind farm performance and influencing parameters, this paper aims to gather relevant information about designing farms, extending the investigation to wind farms with a larger number of turbines in order to observe the effect on turbine efficiency.

For this purpose, in the first part of the study a two-dimensional model of a single turbine is compared with experimental data [23] and three-dimensional numerical [9] results. In the second part, a linear array of Savonius turbines is studied and the role of the distance between adjacent turbines, wind incidence angle, and number of turbines is evaluated.

2. Selected benchmark

The Savonius turbine has been previously investigated using an experimental approach, analyzing fluid dynamic characteristics via tracking technique [24], evaluating geometrical parameters such as the number of blades, the height and number of stages [23,25], and evaluating the effect of the end plates [26,27]. The optimal size of the plate was defined as equal to 1.1 times the diameter of the turbine [27], and the optimal number of blades equal to 2 [25]. Furthermore, optimization through the use of deflectors and different blade profiles was proposed [28–30], increasing efficiency by up to 38.5%. Numerical studies about the turbine performance are also present in literature, focusing on the influence of the overlap in two-dimensional models [31,32].

Valuable data for CFD model validation are available from the wind tunnel test campaign performed by Blackwell et al. [23]. They considered a two-bucket Savonius turbine with an overlap ratio (O.R. = o/d) equal to 0.2, and with geometry parameters listed in Table 1 and Fig. 1. This geometry was studied by Ferrari et al. [9], who tested different wind turbine aspect ratios with a three-dimensional modeling approach. The three-dimensional study is used here to validate the two-dimensional results, analyzing performance differences and turbine tip effects.

Table 1
Geometrical parameters.

Turbine category	Vertical Axis Wind Turbine
Number of buckets	2
d (m)	0.5
D (m)	0.9
s (m)	0.002
o (m)	0.1023
O.R.	0.2

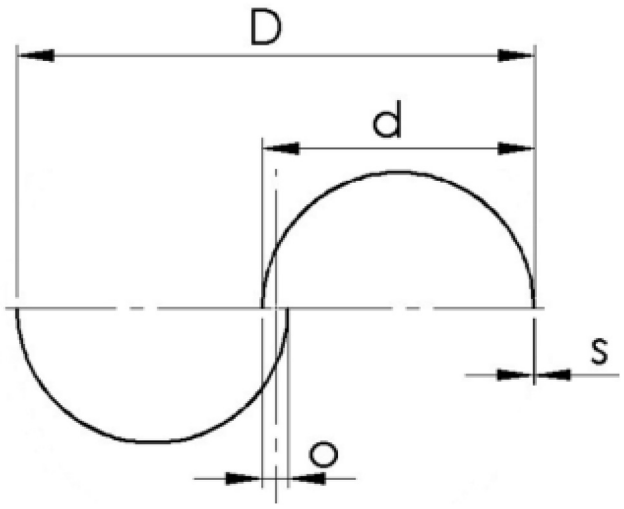

Fig. 1. Schematic geometry of the turbine.

2.1. Performance parameters

In order to compare performance and main fluid-dynamic characteristics, the dimensionless parameters related to torque, power, drag and lift are defined and used.

The dynamic torque coefficient C_m and the power coefficient C_p generated by Savonius turbines are defined as:

$$Cm = \frac{M}{\frac{1}{4}\rho U_{inf}^2 D};\ Cp = \frac{P}{\frac{1}{2}\rho A U_{inf}^3} \tag{1}$$

where A is the frontal area of the turbine, D is the diameter and U_{inf} is the free-stream wind velocity. M is the dynamic torque and P is the power produced. Furthermore, the longitudinal drag C_d and lateral lift C_l coefficients are monitored:

$$Cd = \frac{Drag}{\frac{1}{2}\rho A U_{inf}^2};\ Cl = \frac{Lift}{\frac{1}{2}\rho A U_{inf}^2} \tag{2}$$

The power coefficient, C_p, presented in Eq. (1), is used to identify the grid convergence in Section 3.2.1 and to evaluate the wind turbine performance in Section 6. This coefficient represents the fraction of extracted power over the total available from the free-stream wind blowing through the projected area of the turbine at velocity U_{inf}.

3. Geometrical modeling

This section describes the numerical domain and lateral boundary conditions, in addition to geometrical modeling and grid generation. Furthermore, a sensitivity analysis of the mesh is reported.

3.1. Numerical domain

A two-dimensional numerical domain reproducing the Savonius turbine(s) cross section and the surrounding environment is used in this study. The model represents a turbine characterized by uniform cross section and infinite height. The domain is divided between turbines and environment, with specific interconnecting boundary conditions between them, to model the rotating turbines. This is realized through a moving frame, permitting the use of different grid refinements for turbine region and environment.

Based on the number and distribution of turbines, the size of the numerical domain has to be adapted, maintaining a minimum distance between turbines and boundaries. The numerical domain is built defining a minimum distance between inlet and turbine(s), outlet and turbine(s), and lateral boundaries and turbine(s), depending on the typology of lateral boundary conditions.

The solver used in this study is intrinsically three-dimensional, and to perform a two-dimensional analysis, a domain including the third direction was used. The height of the turbine (H) was set equal to the third dimension size ($H = 0.05\ m$).

Two approaches for modeling lateral boundaries were used: the cyclic approach, which permits limiting the number of modeled turbines to one, therefore simulating an infinite turbine array and without taking into account the wind farm border effects; the discrete approach, which permits modeling of the exact number of turbines, taking into account the border effects.

3.1.1. Cyclic approach

The Cyclic boundary condition approach, also known as the Periodic boundary conditions approach, treats the two lateral boundaries as if they were physically adjacent, with the fluid flow exiting through a boundary entering through the other, and vice-versa. Using this approach, the domain extends for 9D upstream and 17D downstream of the turbine, and the lateral size of the domain is set equal to the required distance between two adjacent turbines L, with the lateral boundary representing the midpoint between two turbines in a virtual infinite array farm, as shown in Fig. 2.

3.1.2. Discrete approach

Differently to the Cyclic approach, lateral boundaries are set as Symmetry, with the normal velocity equal to zero and the necessity to have a distance between turbine and boundary that is enough to avoid flow field perturbation. Domain size was set in order to maintain a distance of at least 20D from the nearest turbine in each direction and the distance between adjacent turbines equal to L, as shown in Fig. 3. A sensitivity analysis of the lateral domain size was performed, to verify the independence of the fluid flow on lateral boundary conditions. A distance of 20D between the turbine array and the lateral boundary was observed to be enough to totally recover the undisturbed inlet velocity U_{inf}. The lateral distance effect was tested for the most critical configuration, with an array of 16 turbines, as reported in Fig. 9.

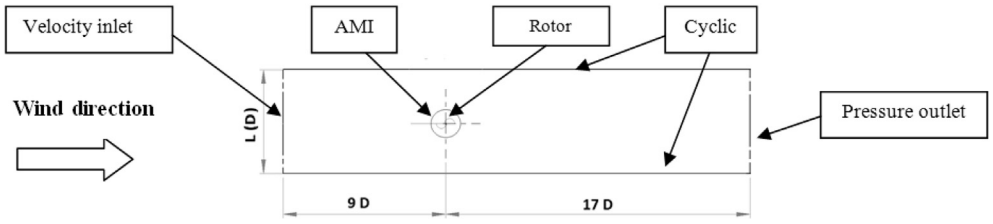

Fig. 2. Domain of the cyclic approach and boundary conditions.

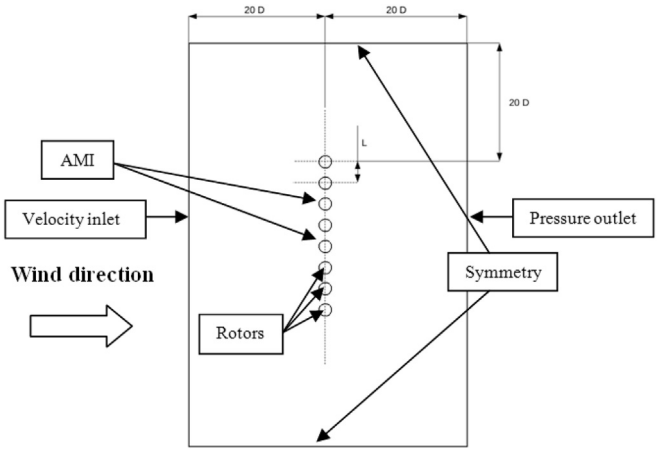

Fig. 3. Domain of the discrete approach.

3.2. Mesh generation

The grid was created using the tools *blockMesh* and *snappyHexMesh* (both available in the native version of OpenFOAM), generating mainly exahedral elements and a local refinement close to the turbine surface. The maximum height of the cells around the turbine surface was set to obtain an average $y^+ = 0.5$, with minimum and maximum values equal to 0.02 and 7.8 (in $< 2\%$ of cells), respectively. Eight layers of prismatic elements, with a growth ratio of 1.2, were set over the blade surface to control the value of y^+, which depends on the local velocity of the fluid flow near the turbine surface. The size of the layers over the blade surface and the cell size around the turbine play a crucial role in simulation accuracy [33]. Even if the domain sizes are different for cyclic and discrete approaches, the grid used in the near-turbine region has the same resolution, while in the discrete approach domain the dimension of the cells is reduced in the region between the turbines and the wake zones. In Fig. 4, the mesh for cyclic (a) and discrete (b) approach domains is reported, with a focus on the region close to the turbine blades (c). The grid size for cyclic and discrete approaches is reported in Table 3 and the grid size for the discrete approach, with $L = 5D$ and the number of turbines ranging from 2 to 16, is reported in Table 4.

3.2.1. Mesh sensitivity analysis

A mesh independence analysis was carried out on the single-turbine configuration using a domain with $12D$ width and symmetry as lateral boundary conditions. This grid was progressively refined until the observed physical quantities became constant. The mesh was evaluated by doubling and halving the number of cells in each direction. The results obtained from grids A, B, and C are reported in Table 2, where no significant variation in the torque coefficient can be observed. Grid C was selected as the right trade-off between computational-time requirement and accuracy, with a difference $< 1\%$ with respect to fine mesh A. Grid C was used for all the analyses reported in Section 6.

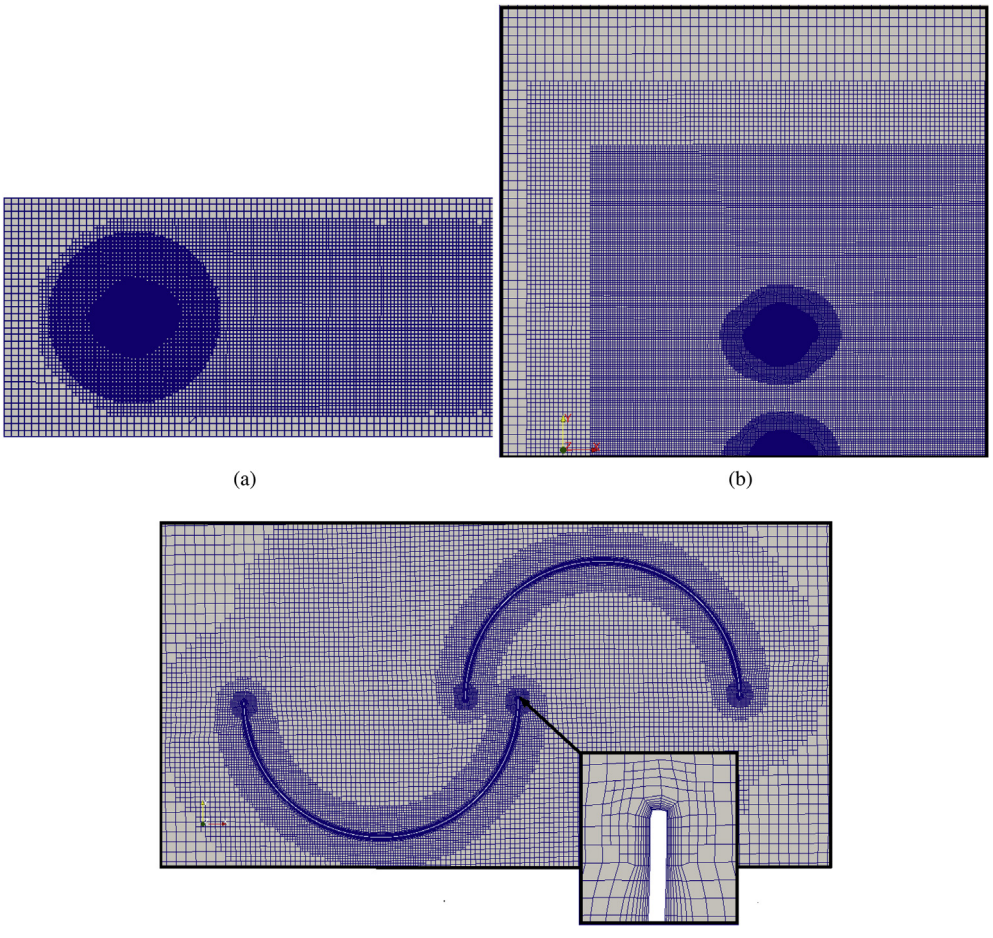

Fig. 4. (a) Cyclic Grid (b) Discrete approach grid (c) Particular of the mesh near blades.

Table 2
Grid analysis.

Name	Cells	TSR	Cm	Cp	Err.	Cd	Err.	Cl	Err.
A	578575	0.81	0.311	0.252	–	1.143	–	−1.059	–
B	159999	0.81	0.311	0.252	0.03%	1.142	0.08%	−1.066	0.66%
C	51000	0.81	0.313	0.254	0.61%	1.139	0.27%	−1.052	0.71%

Table 3
Cyclic and 8 turbines meshes size.

Mesh type	Cyclic approach [Cells]	Discrete approach [Cells]
2D	36700	659000
3D	41000	728000
4D	44500	809000
5D	45600	890300

Table 4
5D spacing discrete meshes.

Mesh type	Number of Cells
2 turbines	432000
4 turbines	584600
8 turbines	890300
16 turbines	1545600

4. Numerical modeling

In this section, a numerical set-up is reported describing the turbulence solver, the boundary and operating conditions, and the numerical methods used for the analysis [34].

4.1. Turbulence modeling and solver

Governing equations for incompressible turbulent flow are modeled via the URANS approach, using an Unsteady Reynolds-Averaged version of mass and momentum (Navier-Stokes) balance equations and transport equations for turbulence quantities. Based on the turbulence model analysis performed in Ref. [9] for three-dimensional modeling and [35] for two-dimensional modeling, the two-equation eddy-viscosity model $k-\omega$ *SST* [36] was selected. This model ensures good behavior in adverse pressure gradients and separating flows, which are found to occur in flows around bluff bodies, such as the Savonius turbine. Transient simulation, including the rotating turbine, is performed using the dynamic type solver *pimpleDyMFoam*, natively implemented in the open source OpenFOAM code release 2.3. This uses a hybrid PISO-SIMPLE (PIMPLE) algorithm for coupling pressure and velocity, allowing the use of larger time steps with respect to the classic PISO algorithm. This method gives the convergence at each time step, using inner loops and a less restrictive Courant-Friedrichs-Lewy (CFL) condition (CFL > 1). The necessary accuracy is guaranteed by the method using a maximum CFL <5.

4.2. Boundary conditions

Referring to the numerical domain previously described in Section 3.1, the boundary conditions are applied to the inlet, outlet, lateral, front and back sides and to the interface between the static and the moving grid, representing the Savonius turbine. All cases refer to the benchmark conditions described in Section 2, considering the Reynolds number ($Re = U_{inf}D/\nu$) as being to $3.9 \cdot 10^5$ with the cinematic viscosity $\nu = 1.62 \cdot 10^{-5}\ m^2/s$ and the turbine diameter $D = 0.9023m$.

The inlet, outlet, front and back boundary conditions and turbine interface type for the communication between the static and the moving grids are the same for both approaches, as reported in Figs. 2 and 3 for Cyclic and Discrete approach, respectively:

- *inlet*: free stream velocity $U_{inf} = 7\ m/s$ with a turbulent intensity $I = 1.4\%$, equivalent to the value measured in the wind tunnel [23];
- *outlet*: pressure gradient equal to zero;
- *front, back*: empty type, guaranteeing to solve equations in two dimensions by specifying the special empty condition on each boundary whose plane is normal to the third dimension for which no solution is required;
- *turbine interface*: AMI (Arbitrary Mesh Interface) type interface, guaranteeing a rigid motion with constant angular speed.

For lateral sides, the boundary conditions are different and set as described in Section 3.1.1 and 3.1.2.

4.3. Numerical schemes

The same discretization schemes were used for all simulations in this study:

- *first and second time derivative terms*: a Bounded First Order Implicit scheme (Euler) was applied;
- *gradient terms*: a second order linear scheme with Gaussian integration for pressure and velocity fields;
- *divergence terms*: a second order Linear Upwind Stabilized Transport (LUST) scheme for vector fields in which linear upwind is blended with linear interpolation to stabilize solutions while maintaining second-order behavior. The scheme is particularly successful in complex geometries with unstructured meshes, e.g. external aerodynamics of vehicles. A second order linear-upwind scheme with Gaussian integration for turbulence quantities was applied;
- *laplacian terms*: a second order linear scheme with Gaussian integration was used.

A linear scheme was used for the interpolation of values from cell centers to face centers.

5. Single turbine two-dimensional modeling validation

In this section, the two-dimensional single turbine configuration is validated with the experimental benchmark of Section 2. The results of the two-dimensional numerical model presented in 3.1 are compared with the three-dimensional numerical results obtained in Ref. [9].

5.1. Two-dimensional numerical modeling vs experimental data

In Fig. 6, the results of the two-dimensional computational model are compared with the experimental data collected during an experimental campaign performed by Sandia Laboratories [23] and based on the geometry described in Section 2.

The performance parameters were calculated from measurements carried out using a turbine of height H = 1 m, aspect ratio 1.1 and in the presence of end-plates.

Dynamic torque and power coefficients show an over-estimation of a two-dimensional numerical model for all analyzed TSR, with the maximum power point translated at higher TSR values. Besides the evident over-estimation of the numerical model, a coherent trend of the coefficients is observed in the range of analyzed TSRs.

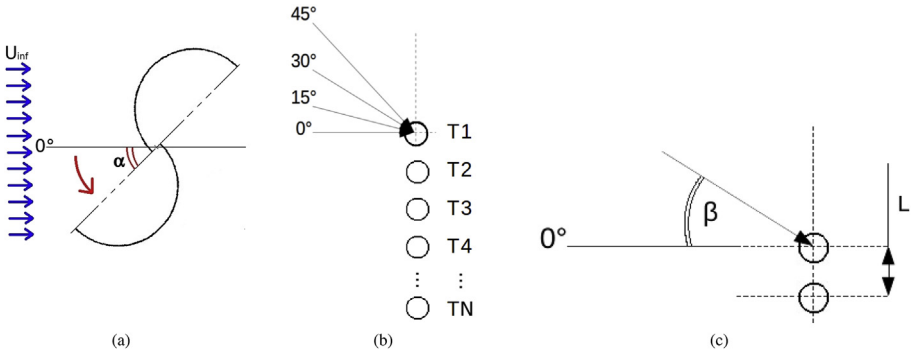

Fig. 5. (a) Turbine angular position; (b) wind direction; (c) nomenclature of the turbines.

5.2. Two vs three-dimensional numerical modeling

In Fig. 7, two and three-dimensional numerical modeling of the single Savonius turbine are compared using dynamic torque and power coefficients. The three-dimensional numerical model is able to correctly detect the maximum power, slightly underestimating the magnitude with respect to experimental data, as reported in Ref. [9].

This comparison shows the importance of three dimensional effects on turbine performance and fluid dynamic behavior, confirming that turbines with and without end plates behave in a different way. The configuration without end plates shows a worse performance and maximum power at lower TSR values. The plates at the end of the blade limit the creation of three dimensional structures at the tip of the blade, and this effect is reproduced by a two-dimensional model with the total absence of these structures. The over-estimation of two-dimensional modeling results (for the turbine with TSR = 0.81) highlights the importance of the third dimension in numerical modeling. Despite the over-estimation, the results can be considered physically correct and able to give an indication of the performance trend for the single turbine.

This difference can be more evident and should be taken into account when evaluating configurations with adjacent turbines, such as finite and infinite turbine arrays. The blockage effect caused by adjacent turbines was previously studied using the three-dimensional numerical modeling approach by Nishino and Draper [37], showing how the presence of other turbines can influence the flow field and related performance. This behavior is further analyzed in this study (Section 6) using two-dimensional modeling.

6. Results and discussion

This section is focused on the analysis of numerical results obtained from Savonius turbine interaction composing a wind farm. In the wind farms, several parameters can influence the flow field hitting the turbines, affecting related performance and global energy production. Among the parameters influencing the performance of the single turbine and wind farm such as farm design, distance between turbines, number of turbines, wind incidence angle and working machine point, the following have been selected and analyzed here, comparing different solutions:

- inter-axial distance;
- wind incidence angle;
- number of turbines.

All the turbines were modeled with a two-dimensional approach, considering the same phase and angular speed and the same TSR= 0.81. In Fig. 5(a) the convention used for the angular position of the single turbine during turbine revolution is shown. Wind turbines are arranged in line with the nomenclature shown in Fig. 5(b). In particular, the first turbine is always windward when the angle of the wind direction is greater than zero. The separation between the turbines, *L*, is expressed as a function of the turbine diameter (D), as shown in Fig. 5(c).

The first part of the section concerns performance at different distances between two adjacent machines and at different wind incidence angles. For this purpose, a cyclic and an 8-turbine discrete approach were simulated comparing performance coefficients and average velocity. The second part investigates the

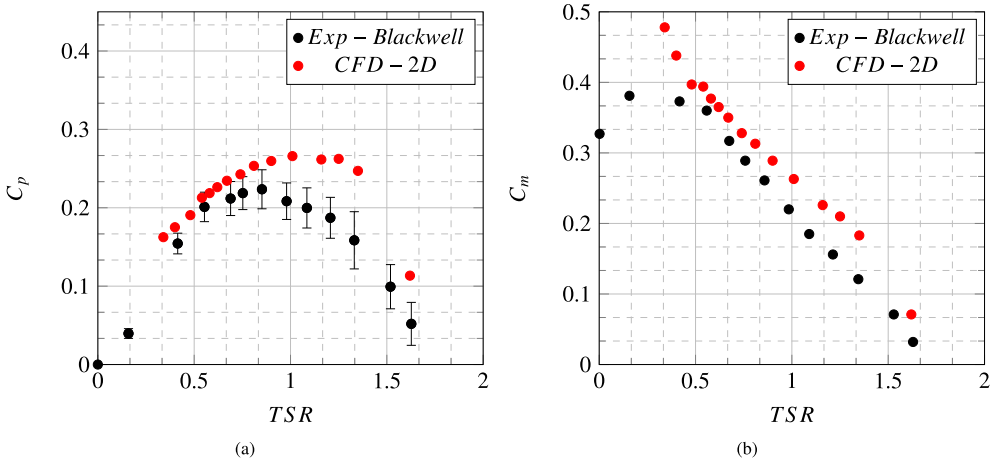

Fig. 6. (a) Cp obtained by two-dimensional model and experimental data from Blackwell. (b) Cm obtained by two-dimensional model and experimental data from Blackwell.

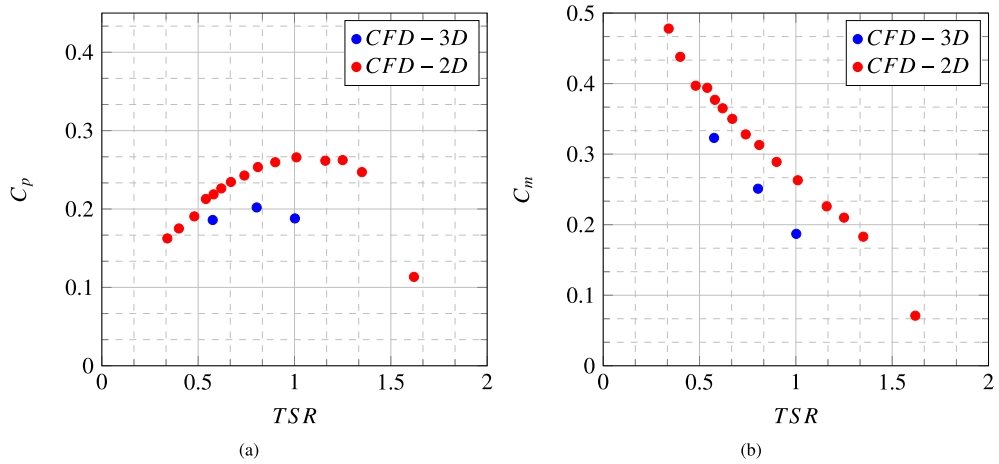

Fig. 7. (a) Cp obtained by two-dimensional model, three-dimensional model (H = 1 m) computational models and experimental data from Blackwell. (b) Cm obtained by two-dimensional model, three-dimensional model computational models and experimental data from Blackwell.

influence of the number of machines, ranging from 2 to 16, with an incident wind angle $\beta = 0^\circ$ and inter-axial distance, L, equal to 5D. Finally, the cyclic boundary conditions approach is used to evaluate the performance of an infinite number of turbines in a linear array.

6.1. Inter-axial distance effect

The simulations for this analysis were conducted with $\beta = 0^\circ$, using both discrete and cyclic approaches, and comparing the results as a function of the distance between axial turbines.

The performance of each turbine (numbered from 1 to 8) for different turbine distances was evaluated, observing the increase of the power coefficient C_p while reducing the turbine distance, regardless of the location in the array, as shown in Fig. 8. The turbine achieving the maximum C_p value in the array depends on the distance between the machines. In the scenario with an inter-axial distance equal to 5D, the most efficient turbine is located in the middle of the array, in the position indicated as #5; for a distance of 4D this is located in position #6 and, for a distance of 3D, in position #7. Finally, in the configuration with a distance of 2D, the peak is positioned at the end of the array.

For all configurations, the fluid flow results are not symmetric with respect to the center of the array. The distribution of the upstream and downstream flows is also not symmetric, because of the direction of rotation for all turbines. In fact, the vortices and fluid structures generated by advancing and returning blades are different, and the interaction effect is affected by the sense of rotation of the turbines.

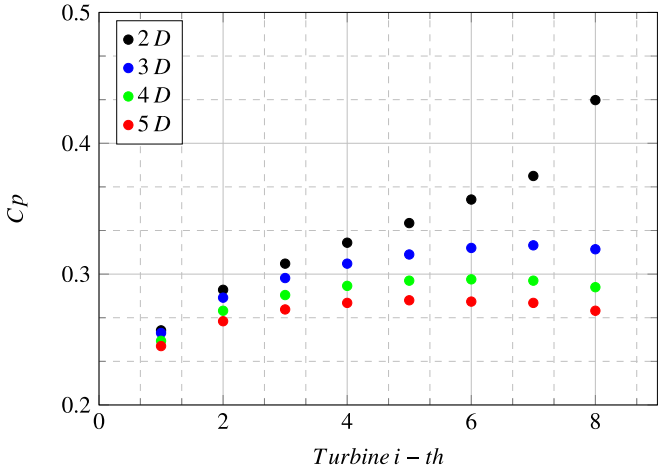

Fig. 8. Comparison of performance in clusters composed of 8 turbines with wind incidence angle 0°.

This behavior is confirmed observing the average flow field at different distances upstream of the turbine farm and the velocity field around adjacent turbines. Additionally, the limited number of turbines does not make it possible to consider the central turbine of the array as being independent from the tail effect. In Fig. 9 the velocity profile at different distances upstream of turbine array is reported for the whole numerical domain. This shows the effect of turbine presence on undisturbed wind velocity and the reduced space necessary for its recovery in a lateral direction around the farm. The velocity magnitude fields reported in Figs. 10 and 11 show a more general overview of the velocity field and interaction between adjacent turbines, highlighting the independence of the velocity upstream of turbines from the inlet boundary conditions and the mutual influence in the wake evolution when compared with a single turbine configuration. The turbulent kinetic energy field of the same wind farm configuration is reported in Fig. 12, where a constant value can be observed upstream of the turbines, while the turbulence varies immediately downstream, coherently with wake evolution. A slightly lower maximum value for the lateral turbines can be also identified, and be related to the differences observed in the velocity trend of Fig. 9.

In order to better understand the effect of a finite number of turbines, the power coefficient calculated with the cyclic approach is compared with the maximum and average values obtained from the discrete approach (eight-turbine configuration), as shown in Fig. 13 and Table 5. The difference among the three curves decreases as the distance between the turbines increases. Therefore, closer machines are more affected by a finite number size of the cluster, with the peak and mean values for 5D configuration remaining below a 3% difference with the cyclic approach, while the 2D configuration reaches a difference up to 29% (see Tables 6–8).

The cyclic approach is hence used to exclude the tail effect in the evaluation of the C_p as a function of the turbine distance, as shown in the polar chart of Fig. 14, where all polar patterns are characterized by 180° symmetry. The reported power trends change, varying the distance between the turbines: at greater distances (i.e. 4D and 5D) the maximum point of production is observed when the turbine is at 20°, while decreasing the inter-axial distance to 3D results in the appearance of a second peak at 45°. By reducing the distance further to 2D, the second peak becomes the only one present, but shifted to 60°.

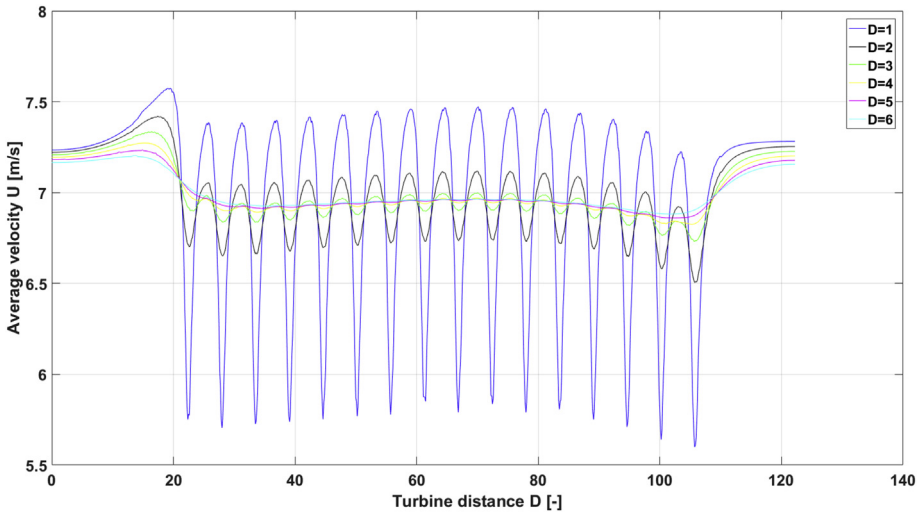

Fig. 9. Average velocity at several distance in front of wind farm.

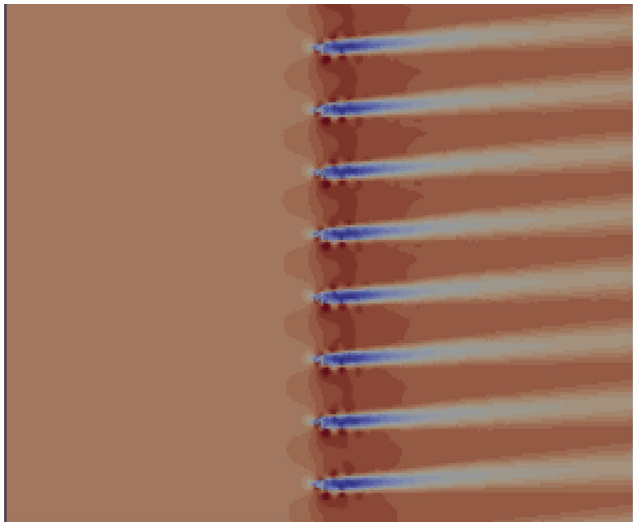

Fig. 10. Magnitude velocity field of eight central turbines of 16-turbine wind farm (min 0 m/s - max 10 m/s).

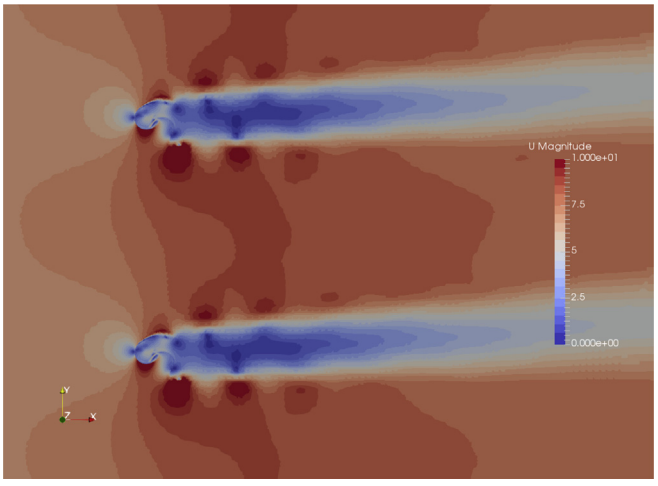

Fig. 11. Magnitude velocity field of two adjacent turbines of wind farm.

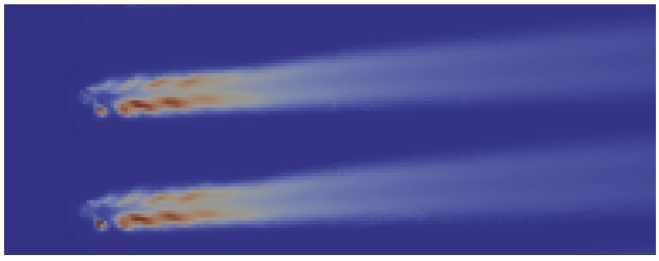

Fig. 12. Turbulent kinetic energy field of two adjacent turbines of wind farm (min 0.00025 - max 4.85 m^2/s^2).

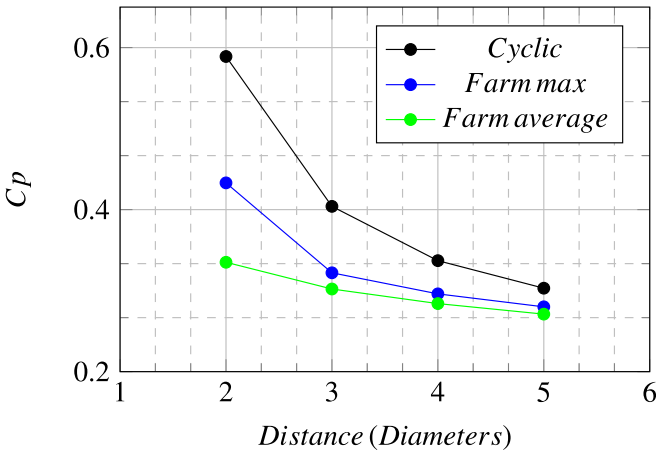

Fig. 13. Mean and maximum power coefficient of discrete and cyclic case, at wind incidence angle 0°.

In Fig. 15 (a) the lift coefficient value is reported as showing a higher maximum for the case at distance 2D and a similar minimum value for all cases. A more evident influence of the turbine distance is observed for the drag coefficient, with an evident increase ranging from configurations 5D to 2D and a rotation of the maximum point from 60° to 90°, as shown in Fig. 15 (b).

6.2. Wind incidence angle effect

In this section the influence of different wind incident angles

Table 5
Mean and maximum power coefficient of discrete and cyclic case.

Case	2 D	3 D	4 D	5 D
Mean discrete Approach	0.335	0.302	0.284	0.271
Maximum discrete approach	0.433	0.322	0.296	0.280
Cyclic	0.589	0.404	0.337	0.303

Table 6
Mean power coefficient as function of wind incident angle.

Distance	0°	15°	30°	45°
2 D	0.335	0.324	0.308	0.272
3 D	0.302	0.295	0.281	0.262
4 D	0.284	0.280	0.269	0.254
5 D	0.271	0.268	0.259	0.247

(i.e. 15°, 30° and 45°) on an eight-turbine array with different turbine distances is evaluated. This analysis cannot be performed with the Cyclic approach, therefore only the Discrete approach is applied here.

The performance of the individual turbines is evaluated varying the wind incident angle from 15° to 45°, as reported in Fig. 16 (a), (b) and (c). The configuration with distance 2D shows a worse power coefficient for the first turbines of the array when compared with other configurations while an evident increase trend is noticed for turbines positioned in the back part of the array. Furthermore, it is possible to note how the turbines with different spacing return similar performances in different positions moving from position #1 to #3 for wind incidences from 15° to 45°, respectively. In Fig. 17, the average performance of the turbine array at different turbine distances is shown as a function of the incidence angle. As the angle increases, the performance of the wind farm significantly decreases in the 2D configuration at 45°, reporting a loss of 19% in efficiency, compared to the 0° condition. This performance deterioration is progressively limited as the distance between adjacent turbines grows.

Considering a wind farm with limited space, such as in an urban environment, the possibility of increasing the number of installed turbines is very important. In order to maximize power and efficiency, statistics about wind direction have to be taken into account, and the possible configurations carefully evaluated. Based on the present analysis and on the fact that power values consistently decrease for closer turbines when the wind incidence angle is 90°, with the windward turbine totally obscuring the rest of the array, as reported by Golecha et al. [38], if a main direction of the wind is identified, it is convenient to place the farm perpendicular to that direction (i.e. 0°). Finally, it is important to highlight how almost all configurations maintain an efficiency advantage compared to the single turbine, excluding 5D configuration with wind at 45°, in which the performance loss is 3% compared with the single turbine configuration.

6.3. Number of turbines effect

This section is dedicated to analyzing the effect of machine numbers on wind farm efficiency. The main purpose is to compare Cyclic and Discrete approaches in order to understand if the difference in productivity lies in the size of the simulated farm. Indeed, when the number of turbines simulated with the discrete approach increases, the results of the two approaches converge. For this analysis a 5D spacing and 0° wind configuration incidence was used.

6.3.1. Performance parameters

The evolution of the efficiency of each turbine is reported in Fig. 18, varying the total number of the turbines in the farm. With a two-turbine configuration, the productivity of the downstream machine is higher than that of the first one, Fig. 18 (a), while in a four-turbine cluster the productivity variation between two adjacent turbines decreases, decreases as the tail of the array approaches, Fig. 18 (b), with the absence of symmetry between the two extremes of the array. The situation evolves for the eight-turbine and sixteen-turbine configurations, with the latter showing a parabolic performance trend with the peak at the center of the array, as shown in Fig. 18 (d).

Table 7
Evolution of mean and maximum power value as function of farm number of turbines.

Case	Max C_p	Mean C_p
2 Turbines	0.246	0.239
4 Turbines	0.258	0.250
8 Turbines	0.280	0.271
16 Turbines	0.294	0.284
Cyclic	0.303	–

6.3.2. Drag and lift coefficients

The drag and lift coefficients of each turbine in a sixteen-turbine configuration are reported in Fig. 19 (a) and (b), respectively. The drag coefficient shows a parabolic trend with higher values for the cyclic approach, coherently with the power coefficient curve of Fig. 18 (d). The performance of the lift coefficient increases in magnitude with a wide stable region in the central part of the array (from the turbines in positions #5 to #12). The most important changes in this parameter are observed in the machines at the end

Table 8
Drag and Lift coefficient evolution as function of turbine number.

Case	Maximum C_d	Mean C_d	Maximum C_l	Mean C_l
2 Turbine	1.11	1.10	−1.07	−1.02
4 Turbine	1.18	1.16	−1.12	−1.05
8 Turbine	1.26	1.22	−1.15	−1.07
16 Turbine	1.33	1.29	−1.15	−1.10
Cyclic	1.38	–	−1.09	–

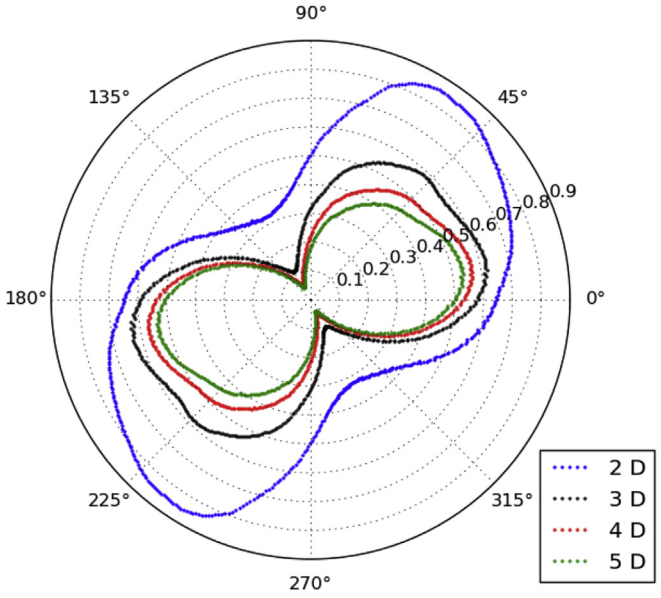

Fig. 14. Power coefficient vs turbine distance for the cyclic approach.

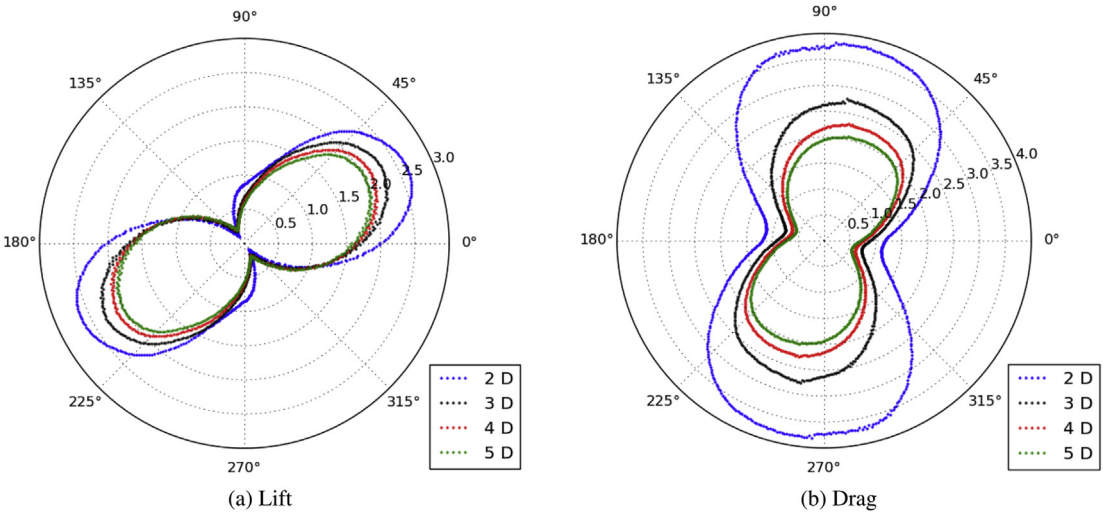

Fig. 15. Drag and lift coefficient vs turbine distance for the cyclic approach.

of the cluster. The turbine in position #1 has a lower efficiency than that in position #16, although having higher values of longitudinal force. This can be explained by the different balance between drag and lift for the turbines composing the array.

6.3.3. Configuration effect

As shown in Fig. 20, the maximum value of turbine efficiency depends on the number of turbines. By increasing the wind farm size, the performance of the best turbine in the cluster tends asymptotically towards the upper limit calculated by Cyclic approach. This demonstrates the coherence between the two different approaches and confirms the results obtained by both of them. Fig. 20 also shows the average performance value of both configurations, varying the number of turbines, with the presence of an asymptotic trend, although the difference between the Cyclic and the Discrete approach is not negligible (see Fig. 21).

Both drag and lift coefficients confirm the consistency of the approaches used here, with the drag coefficient of the Discrete approach showing a clear asymptotic trend for both average and maximum values, tending to the Cyclic approach limit. In fact, the

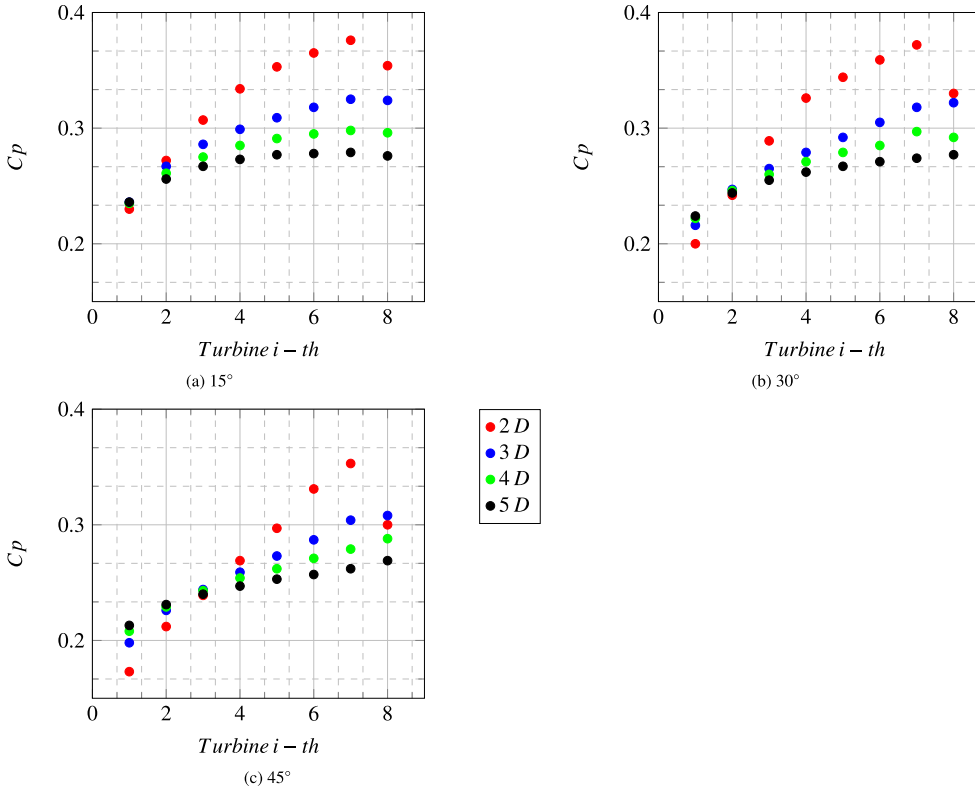

Fig. 16. Comparison of performance in clusters composed of 8 turbines as function of wind incidence angle.

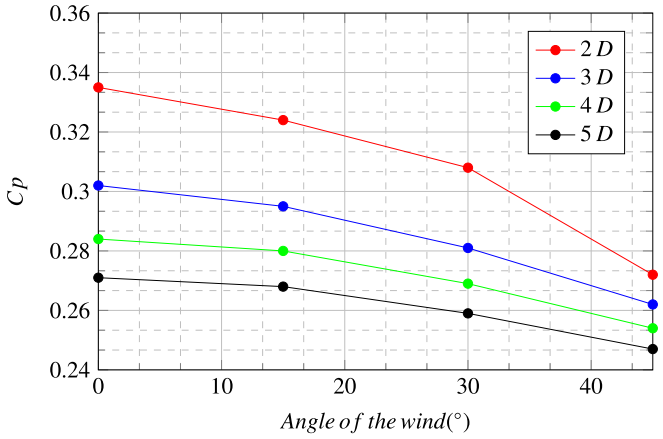

Fig. 17. Mean efficiency value as function of wind incident angle.

difference between the maximum value and the cyclic one changes from 19.6% for the two-turbine configuration to 3.6% for the sixteen-turbine one. The difference in the maximum lift for a configuration over the comparison with the cyclic approach is less than 5% for each array size, confirming the comparability of the two approaches. For all analyzed cases reported in this section, the influence of the blockage effect, observed comparing single and multiple turbine configurations, is evaluated. The two-dimensional approach permits evaluation of the lateral blockage effect, without take into account the influence of the third dimension in the quantitative evaluation of turbine performance. Referring to Nishino and Draper [37], an evaluation of the third-dimension effect can be included, in order to better estimate the performance increase for turbine arrays, even if they limit the analysis to a narrow turbine configuration with a $0.5D$ lateral and vertical gap between adjacent turbines and ground, respectively.

7. Conclusions

Savonius turbines are investigated as a valid alternative for distributed power generation in urban areas. The main factors influencing the farm performance, design and size, are studied.

For this purpose, a two-dimensional modeling approach is applied to the selected benchmark, and the results for the single turbine are compared with available experimental data and the numerical results carried out with a three-dimensional model. The present two-dimensional approach is able to reproduce the trend of the turbine performance, but an overestimation of 20% in turbine efficiency is observed, if compared to the three-dimensional

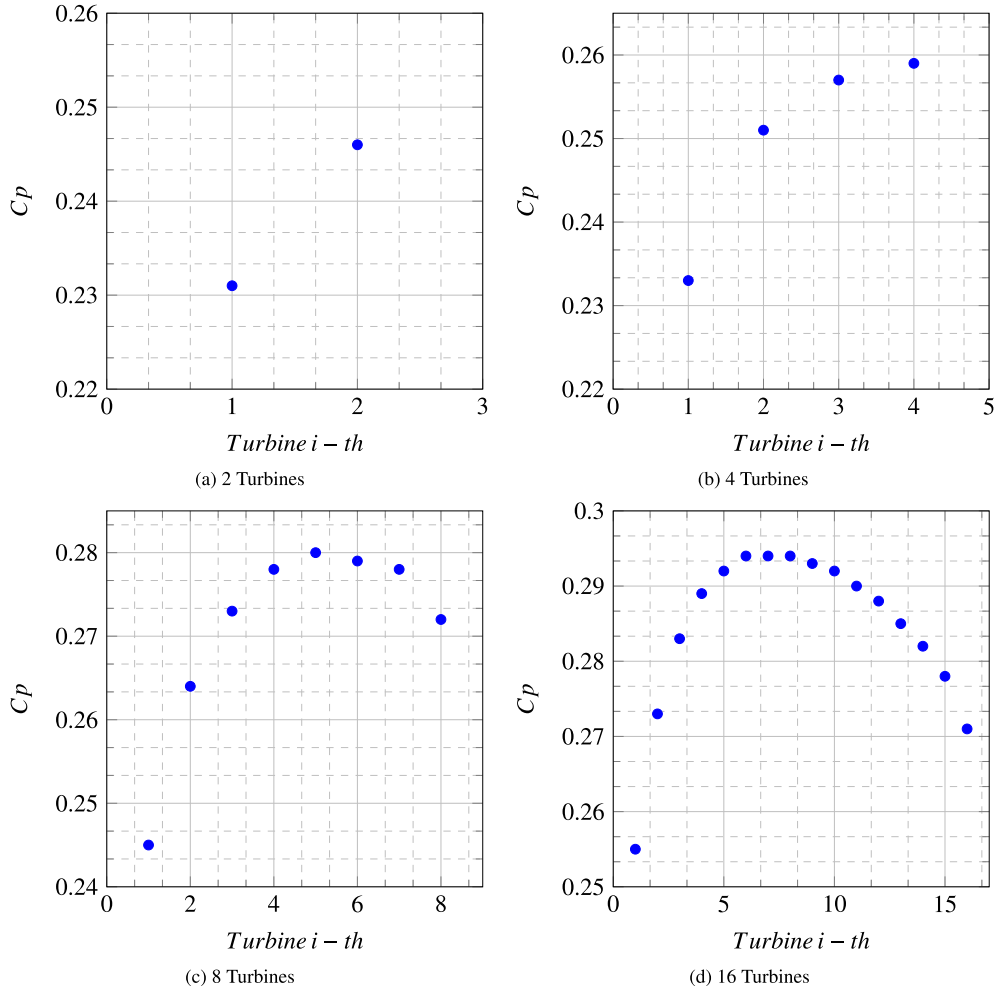

(a) 2 Turbines

(b) 4 Turbines

(c) 8 Turbines

(d) 16 Turbines

Fig. 18. Power coefficient as function of farm number of turbines.

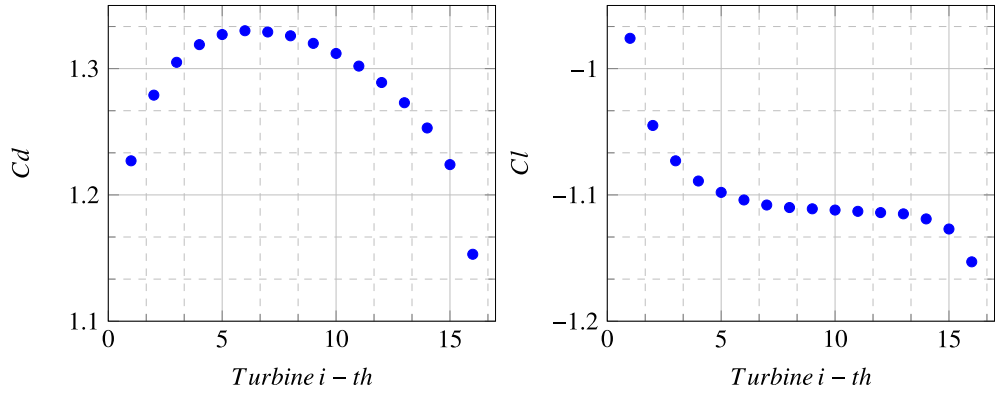

(a) (b)

Fig. 19. Drag and Lift Coefficient of single turbine, 16 turbine case.

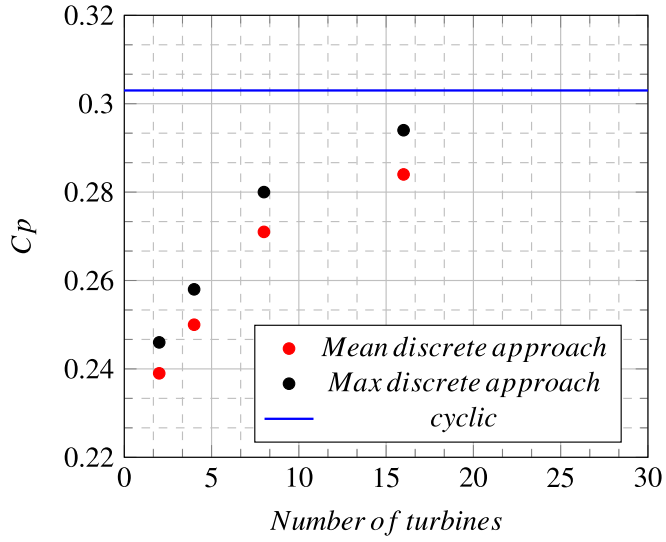

Fig. 20. Evolution of mean and maximum power value as function of farm number of turbines.

results. This is related to the simplification of the flow resolution in the present modeling approach, where the typical tip effects of the turbines with limited aspect ratio are neglected.

The modeling approach was applied to study the interaction of multiple Savonius turbines in a linear array configuration, composed of from 2 to 16 turbines.

The effects of the distance between adjacent machines were evaluated, showing that a cluster of Savonius turbines has a higher efficiency with closer turbines, improving the global performance of the farm. This aspect is very important in urban areas, where the available space is an issue.

The wind incidence angle was also investigated, showing for all configurations lower performance when the incidence angle was greater than zero degrees, independently from the distance between adjacent turbines. This aspect assumes an important role during the definition of the wind array orientation and the evaluation of potential constraints.

Finally, the number of turbines was varied, observing an increase of 19% in farm efficiency when the number of turbines was increased from 2 to 16.

This study gives an estimation of the reliability and approximation introduced using a two-dimensional CFD modeling

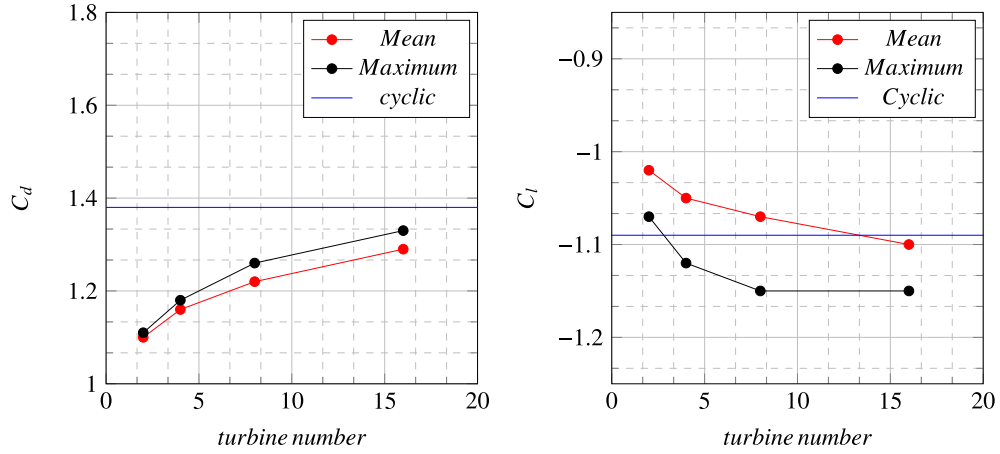

(a) (b)

Fig. 21. Drag and Lift coefficient evolution.

approach for the evaluation of Savonius turbine performance. Furthermore, the influence of the main parameters governing wind farm performance was analyzed, giving an indication of their importance for efficiency evaluation in practical applications.

References

[1] W.E.C.-G. GLOBAL, Global Wind Report: Annual Market Update, GWEC, Brussels, 2014 [Links].

[2] N. Vaughn, Wind Energy: Renewable Energy and the Environment, first ed., CRC Press, 2009.

[3] S. Sivasegaram, Design parameters affecting the performance of resistance-type, vertical-axis windrotors-an experimental investigation, Wind Eng. 1 (1977) 207–217.

[4] K. Pope, I. Dincer, G. Naterer, Energy and exergy efficiency comparison of horizontal and vertical axis wind turbines, Renew. Energy 35 (9) (2010) 2102–2113.

[5] V. Dossena, G. Persico, B. Paradiso, L. Battisti, S. dell'Anna, A. Brighenti, E. Benini, An experimental study of the aerodynamics and performance of a vertical axis wind turbine in a con?ned and uncon?ned environment, ASME J. Energy Resour. Technol. 137 (5) (2015) 1–12.

[6] L. Battisti, E. Benini, A. Brighenti, M. Raciti Castelli, S. dell'Anna, V. Dossena, G. Persico, U. Schmidt Paulsen, T. Pedersen, Wind tunnel testing of the deepwind demonstrator in design and tilted operating conditions, Energy 111 (2016) 484–497.

[7] G. Persico, V. Dossena, B. Paradiso, L. Battisti, A. Brighenti, E. Benini, Time-resolved experimental characterization of wakes shed by h-shaped and tro-poskien vertical axis wind turbines, ASME J. Energy Resour. Technol. 139 (3) (2017) 1–12.

[8] P. Jaohindy, S. McTavish, F. Garde, A. Bastide, An analysis of the transient forces acting on savonius rotors with different aspect ratios, Renew. Energy 55 (2013) 286–295.

[9] G. Ferrari, D. Federici, P. Schito, F. Inzoli, R. Mereu, Cfd study of savonius wind turbine: 3d model validation and parametric analysis, Renew. Energy 105 (2017) 722–734, http://dx.doi.org/10.1016/j.renene.2016.12.077.

[10] L. Vermeer, J. Soerensen, A. Crespo, Wind turbine wake aerodynamics, Prog. Aerosp. Sci. 39 (2003) 467–510.

[11] P. McKay, R. Carriveau, D.-K. Ting, Wake impacts on downstream wind turbine performance and yaw alignment, Wind Energy 16 (2013) 221–234.

[12] R. Barthelmie, O. Rathmann, S. Frandsen, K. Hansen, E. Politis, J. Prospathopoulos, K. Rados, D. Cabezn, W. Schlez, J. Phillips, A. Neubert, J. Schepers, S. van der Pijl, Modelling and measurements of wakes in large wind farms, J. Phys. Conf. Ser. 75.

[13] R. Barthelmie, S. Pryor, S. Frandsen, K. Hansen, J. Schepers, K. Rados, W. Schlez, A. Neubert, L. Jensen, S. Neckelmann, Quantifying the impact of wind turbine wakes on power output at offshore wind farms, J. Atmos. Ocean. Technol. 27 (2010) 1302–1317.

[14] J. Dabiri, Potential order-of-magnitude enhancement of wind farm power density via counter-rotating vertical-axis wind turbine arrays, J. Renew. Sustain. Energy 3.

[15] M. Kinzel, Q. Mulligan, J. Dabiri, Energy exchange in an array of vertical-axis wind turbines, J. Turbul. 38 (2012) 1–13.

[16] K. Duraisamy, V. Lakshminarayan, Flow physics and performance of vertical axis wind turbine arrays, 32nd AIAA Applied Aerodynamics Conference (2014) 1–17.

[17] M. Ahmadi-Baloutaki, R. Carriveau, D.-K. Ting, A wind tunnel study on the aerodynamic interaction of vertical axis wind turbines in array configurations, Renew. Energy 96 (2016) 904–913.

[18] M. Shaheen, M. El-Sayed, S. Abdallah, Numerical study of two-bucket savonius wind turbine cluster, J. Wind Eng. Ind. Aerodyn. 137 (2015) 78–89.

[19] M. Shaheen, S. Abdallah, Development of efficient vertical axis wind turbine clustered farms, Renew. Sustain. Energy Rev. 63 (2016) 237–244, http://dx.doi.org/10.1016/j.rser.2016.05.062.

[20] B. Belkacem, M. Paraschivoiu, Cfd analysis of a finite linear array of savonius wind turbines, J. Phys. Conf. Ser. 753, http://dx.doi.org/10.1088/1742-6596/753/10/102008.

[21] M. Mohamed, Design Optimization of Savonius and Wells Turbines, Ottovon-Guericke University Magdeburg, 2011.

[22] A. El-Baz, K. Youssef, M. Mohamed, Innovative improvement of a drag wind turbine performance, Renew. Energy 86 (2016) 89–98.

[23] B. Blackwell, R. Sheldahl, L. Feltz, Wind tunnel performance data for two and three bucket savonius rotors, J. Energy 2 (3) (1977) 160–164.

[24] M. Nakajima, S. Iio, T. Ikeda, et al., Performance of double step savonius rotor for environmentally friendly hydraulic turbine, J. Fluid Sci. Technol. 3 (1) (2008) 420–429.

[25] N. Mahmoud, A. El-Haroun, E. Wahba, M. Nasef, An experimental study on improvement of savonius rotor performance, Alexandria Eng. J. 51 (1) (2012) 19–25.

[26] I. Ushiyama, H. Nagai, Optimum design configurations and performance of savonius rotors, Wind Eng. 12 (1) (1988) 59–75.

[27] S. Sivasegaram, Secondary parameters affecting the performance of resistance type vertical axis wind rotors, Wind Eng. 2 (1978) 49–58.

[28] B.D. Altan, M. Atılgan, A. Özdamar, An experimental study on improvement of a savonius rotor performance with curtaining, Exp. Therm. Fluid Sci. 32 (8) (2008) 1673–1678.

[29] K. Tesch, K. Kludzinska, P. Doerffer, Investigation of the aerodynamics of an innovative vertical-axis wind turbine, Flow Turbul. Combust. 95 (4) (2015) 739–754.

[30] M.H. Khan, Model and prototype performance characteristics of savonius rotor windmill, Wind Eng. 2 (1978) 75–85.

[31] N.A. Samiran, A.A. Wahab, S. Mohd, N. Rosly, Simulation study on the performance of vertical axis wind turbine, Appl. Mech. Mater. 465 (2014) 270–274.

[32] J.V. Akwa, G. da Silva Júnior, A. Petry, Discussion on the verification of the overlap ratio influence on performance coefficients of a savonius wind rotor using computational fluid dynamics, Renew. Energy 38 (1) (2012) 141–149.

[33] T. Krysiński, Z. Buliński, A.J. Nowak, Numerical modeling and preliminary validation of drag-based vertical axis wind turbine, Arch. Thermodyn. 36 (1) (2015) 19–38.

[34] E. Colombo, F. Inzoli, R. Mereu, A methodology for qualifying industrial cfd: the q3 approach and the role of a protocol, Comput. Fluids 54 (2012) 56–66.

[35] J. Abraham, G. Mowry, B. Plourde, E. Sparrow, W. Minkowycz, Numerical simulation of fluid flow around a vertical-axis turbine, J. Renew. Sustain. Energy 3 (3) (2011) 033109.

[36] F. R. Menter, Zonal two equation k-turbulence models for aerodynamic flows, AIAA Paper 2906 (1993) 1993.

[37] T. Nishino, S. Draper, Local blockage effect for wind turbines, J. Phys. Conf. Ser. 625 (2015) 1–10, http://dx.doi.org/10.1088/1742-6596/625/1/012010.

[38] K. Golecha, T.I. Eldho, S.V. Prabhu, Study on the interaction between two hydrokinetic savonius turbines, Int. J. Rotating Mac. 2012 (2012), http://dx.doi.org/10.1155/2012/581658. Article ID 581658, 10 pages.

Glossary

H: Height of the turbine (m)
D: Diameter of the turbine (m)
d: Diameter of the blade (m)
s: Thickness of the blade and end plate (m)
o: Distance between the blades (m)
A: Frontal area of the turbine (m^2)
L: Distance between turbines (m)
U_{inf}*:* Freestream velocity of the wind (m/s)
ω*:* Angular velocity (rad/s)
O.R.: Overlap ratio (−)
ρ*:* Density of the air (kg/m^2)
ν*:* Cinematic viscosity (m^2/s)
α*:* Angle of position of the turbine (°)
β*:* Angle of incidence of the wind (°)
P: Power (W)
M: Torque (Nm)
C_p*:* Coefficient of power (−)
C_m*:* Coefficient of momentum (−)
C_d*:* Coefficient of drag
C_l*:* Coefficient of lift
TSR: Tip Speed Ratio (−)
CFL: Courant Friedrichs Lewy number (−)